

## Stabilization of Nuclear Isovector Valence-Shell Excitations

G. Rainovski,<sup>1,2</sup> N. Pietralla,<sup>1,3</sup> T. Ahn,<sup>1</sup> C. J. Lister,<sup>4</sup> R. V. F. Janssens,<sup>4</sup> M. P. Carpenter,<sup>4</sup> S. Zhu,<sup>4</sup> and C. J. Barton III<sup>5</sup>

<sup>1</sup>Department of Physics and Astronomy, SUNY at Stony Brook, Stony Brook, New York 11794-3800, USA

<sup>2</sup>Faculty of Physics, St. Kliment Ohridski University of Sofia, 1164 Sofia, Bulgaria

<sup>3</sup>Institut für Kernphysik, Universität zu Köln, 50937 Cologne, Germany

<sup>4</sup>Argonne National Laboratory, 9700 South Cass Avenue, Argonne, Illinois 60439, USA

<sup>5</sup>Department of Physics, University of York, Heslington, York YO1 5DD, United Kingdom

(Received 27 November 2005; published 30 March 2006)

Excited states in  $^{138}\text{Ce}$  have been studied via the  $^{12}\text{C}(^{138}\text{Ce}, ^{138}\text{Ce}^*)$  Coulomb excitation reaction at 480 MeV. Relative cross sections have been determined from the  $\gamma$ -ray yields observed with Gammasphere. The  $E2$  and  $M1$  strength distributions between the lowest six  $2^+$  states up to 2.7 MeV enables us to identify the  $2_4^+$  state in  $^{138}\text{Ce}$  as the dominant fragment of the one-phonon  $2_{1,\text{ms}}^+$  mixed-symmetry state. Mixing between this level and a nearby isoscalar state is observed and is more than 4 times larger than in the neighboring isotone  $^{136}\text{Ba}$ . This is direct evidence that the stability of mixed-symmetry states strongly depends on the underlying subshell structure.

DOI: 10.1103/PhysRevLett.96.122501

PACS numbers: 21.10.Re, 23.20.Js, 25.70.De, 27.60.+j

Atomic nuclei are examples of mesoscopic two-fluid quantum systems. The physics of these systems is determined by three main properties: the many-body aspect, the quantum nature, and the two-fluid character. Nuclear phenomena that reflect these three properties are collectivity, shell structure, and the isospin degree of freedom. Of particular importance for studying the mutual balance of these aspects are those excitations that are related to the collective two-fluid character of nuclei and to their shell structure. Quadrupole-collective isovector valence-shell excitations, so-called mixed-symmetry states (MSSs) [1], are the best studied examples of this class of phenomena. A special type of MSS, the  $J^\pi = 1^+$  scissors mode, was first discovered in nuclei [2] and was reported or suggested to exist in Bose-Einstein condensates [3] and metallic clusters [4].

The fundamental MSS in collective two-fluid quantum systems with quadrupole residual interactions, such as heavy nuclei, is the one-quadrupole phonon  $2_{1,\text{ms}}^+$  state [1]. Because of its role as a building block of isovector excitations in nuclei, and in quadrupole-collective two-fluid quantum systems in general, it is important to study its properties and the mechanisms that determine those. However, information on MSSs is scarce. Due to experimental challenges, MSSs have been observed so far for stable nuclei only. The best examples are found in the mass  $A \approx 90$  region [5–7], while there are only a few reported cases in the  $A \approx 130$  region below the  $N = 82$  shell closure, e.g., [8–10]. Apparently, to investigate MSSs, new experimental methods, in particular, those that could potentially be applied to radioactive isotopes, are needed.

It is the purpose of this Letter to demonstrate that the observation of  $\gamma$  rays from inverse kinematics Coulomb excitation with a  $4\pi$  spectrometer can identify and probe the  $2_{1,\text{ms}}^+$  state of any vibrational nucleus that can be made available as an ion beam. Here, we study the nucleus  $^{138}\text{Ce}$  which has a natural abundance of 0.25%. The technique is

generic and equally applicable to radioactive beams [11] that can be produced with sufficient intensity ( $\sim 10^6$  ions/s for detailed spectroscopy,  $\sim 10^3$  ions/s for identification). The high selectivity for  $J = 2$  states avoids much traditional searching and reveals the entire  $E2$  strength distribution in a few hours. The data, when compared to the neighboring  $N = 80$  isotone  $^{136}\text{Ba}$  [10], provide first evidence for a direct influence of subshell structure on the properties of the MSSs. This can be viewed as *shell stabilization* of the quadrupole isovector excitations. Microscopic wave functions for the  $2_{1,\text{ms}}^+$  state in  $^{136}\text{Ba}$  have previously been calculated [12] in the quasiparticle-phonon model [13] and support this interpretation.

The experiment was carried out at Argonne National Laboratory. The  $^{138}\text{Ce}$  beam with intensity of  $\approx 1$  pA was delivered by the ATLAS accelerator. The 480 MeV beam was incident on a  $1 \text{ mg/cm}^2$   $^{12}\text{C}$  target. The deexcitation  $\gamma$  rays, following the Coulomb excitation of the projectile, were detected with the Gammasphere array [14] which consisted of 98 HPGe detectors arranged in 15 rings. Gammasphere was used in singles mode resulting in an average counting rate of 4000 counts-per-second (cps), while the room background was producing about 600 cps. A total of  $2.4 \times 10^8$  events of  $\gamma$ -ray fold 1 or higher was collected in about 14 hours.

The contribution of the room background was eliminated in the offline sort by correlating the  $\gamma$  rays with the accelerator radio-frequency (rf) signal. The final spectrum, which is a difference between the “beam-on” (with respect to the rf) spectrum and the “beam-off” spectrum, scaled to eliminate the 1461 keV room background transition from  $^{40}\text{K}$ , is shown in Fig. 1. All  $\gamma$  rays in the spectrum originate from  $^{138}\text{Ce}$  nuclei recoiling with  $v/c \approx 6.9\%$ . Most of these  $\gamma$  rays have already been identified in  $^{138}\text{Ce}$  [15–19]. We have observed two new transitions with respective energies of 1354 and 2143 keV. Because of the Doppler

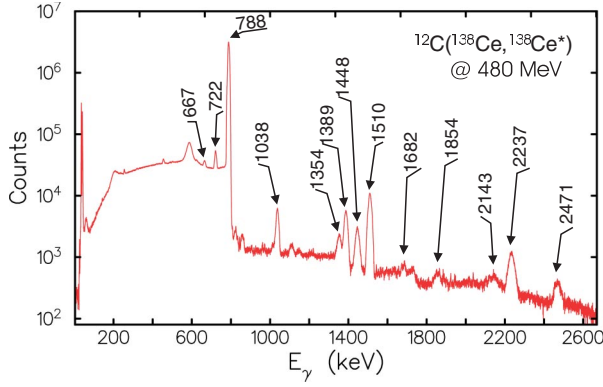


FIG. 1 (color online). Background-subtracted, Doppler-corrected  $\gamma$ -ray spectrum in  $^{138}\text{Ce}$  observed with Gammasphere after Coulomb excitation on a carbon target.

broadening, the energy resolution is 1.4% and translates into  $\gamma$ -ray energy uncertainties of about 1 keV. This excludes the possibility that the new  $\gamma$  rays originated from the decay of the  $4_2^+$  state at 2137 keV. About 3% of the data have  $\gamma$ -ray fold higher than 1. The coincidence relationships suggest that the two new  $\gamma$  rays depopulate a level at 2143 keV in  $^{138}\text{Ce}$ , which is observed here for the first time.

The coincidences further show that any contribution of the 1348-keV,  $4_2^+ \rightarrow 2_1^+$  transition [19] to the peak area of the 1354 keV line is statistically insignificant. The spectroscopic information is summarized in Table I.

The spins of the levels were assigned on the basis of an angular distribution analysis [21]. The intensities of the  $\gamma$  rays were measured over the 15 rings of Gammasphere, corrected for the Lorentz boost [22] and fitted with the angular distribution function [21]. The experimental  $A_2/A_0$  and  $A_4/A_0$  coefficients for the stretched transitions unambiguously determined the  $\gamma$ -ray multipolarity and, hence, the spins of the excited states and their orientations. The latter were used to determine the multipole mixing ratios for the transitions between the excited states, as illustrated in Fig. 2. In the cases where the stretched transitions to the ground state are weak and do not allow for an angular distribution analysis, the orientation parameters from the closest level were used. The results for the mixing ratios are summarized in Table I. The mixing ratio for the 1448 keV transition is small which shows that the  $2_4^+ \rightarrow 2_1^+$  transition is 97(2)% of magnetic dipole character.

In the present experiment, we have observed the decay of the  $0_2^+$ ,  $3_1^-$ , and  $4_1^+$  states, and the first six  $2_{1,2,3,4,5,6}^+$  states up to an excitation energy of 2.7 MeV. The relative  $\gamma$ -ray

TABLE I. Measured properties of the levels and  $\gamma$ -ray transitions in  $^{138}\text{Ce}$  in standard notation.

| $E_{\text{level}}$<br>(keV) | $J^\pi$ | $\tau$ (fs)            | $E_\gamma$<br>(keV) | $I_\gamma$           | $J_{\text{final}}^\pi$ | $A_2/A_0$  | $A_4/A_0$  | $\delta$                    | Transition strength <sup>a</sup>                                      |
|-----------------------------|---------|------------------------|---------------------|----------------------|------------------------|------------|------------|-----------------------------|---|
| 788                         | $2_1^+$ | 2970(200) <sup>b</sup> | 788                 | 10 <sup>6</sup> (97) | $0_1^+$                | 0.112(5)   | -0.003(7)  |                             | $B(E2) = 21.2(14)$ <sup>b</sup>                                       |
| 1476                        | $0_2^+$ |                        | 688 <sup>c</sup>    | 69(6)                | $2_1^+$                |            |            |                             |   |
| 1511                        | $2_2^+$ | 1203(29)               | 1510                | 9682(59)             | $0_1^+$                | 0.201(7)   | -0.056(10) |                             | $B(E2) = 1.16(8)$   |
|                             |         |                        | 722                 | 7328(61)             | $2_1^+$                | -0.172(8)  | -0.018(11) | $-1.97^{+0.32}_{-0.25}$     | $B(M1) = 0.011(2)$<br>$B(E2) = 28(2)$                                 |
| 1826                        | $4_1^+$ |                        | 1038                | 2565(15)             | $2_1^+$                | 0.347(10)  | -0.033(13) |                             |   |
| 2143                        | $2_3^+$ | 177(10)                | 2143                | 378(8)               | $0_1^+$                |            |            |                             | $B(E2) = 0.57(4)$   |
|                             |         |                        | 1354                | 1173(13)             | $2_1^+$                | -0.203(15) | -0.005(15) | $-0.833^{+0.057d}_{-0.076}$ | $B(M1) = 0.058(6)$<br>$B(E2) = 7.5(9)$<br>$B(E3) \uparrow = 0.163(9)$ |
| 2177                        | $3_1^-$ |                        | 1389                | 4103(28)             | $2_1^+$                | -0.191(9)  | -0.006(12) | $-0.025^{+0.012d}_{-0.019}$ |   |
|                             |         |                        | 667                 | 1970(26)             | $2_2^+$                |            |            |                             |   |
| 2237                        | $2_4^+$ | 82(5)                  | 2237                | 1811(25)             | $0_1^+$                | 0.298(21)  | -0.084(27) |                             | $B(E2) = 1.86(16)$  |
|                             |         |                        | 1448                | 2263(15)             | $2_1^+$                | 0.308(14)  | 0.012(18)  | $0.184^{+0.052}_{-0.042}$   | $B(M1) = 0.122(10)$<br>$B(E2) = 0.65(10)$<br>$B(E2) = 0.74(20)$       |
| 2471                        | $2_5^+$ | 157(9)                 | 2471                | 508(13)              | $0_1^+$                |            |            |                             | $B(E2) = 0.74(20)$  |
|                             |         |                        | 1682                | 411(5)               | $2_1^+$                |            |            |                             | $B(M1) \leq 0.034(3)$ <sup>e</sup>                                    |
| 2642                        | $2_6^+$ | 95(46)                 | 2642                | 87(35) <sup>f</sup>  | $0_1^+$                |            |            |                             | $B(E2) = 0.42(8)$   |
|                             |         |                        | 1854                | 250(10)              | $2_1^+$                |            |            |                             | $B(M1) \leq 0.069(47)$ <sup>e</sup>                                   |

<sup>a</sup> $B(E2)$  values are given in W.u. (1 W.u. =  $42.4e^2 \text{ fm}^4$ ),  $B(M1)$  values are given in  $\mu_N^2$ , and the  $B(E3) \uparrow$  value is given in  $e^2 b^3$ .

<sup>b</sup>From Ref. [20].

<sup>c</sup>This transition can only be observed in coincidence with the  $2_1^+ \rightarrow 0_1^+$  transition.

<sup>d</sup>The orientation of the state is assumed to be the same as for the  $2_4^+$  state.

<sup>e</sup>Since the multipole mixing ratio is not measured we assume here  $\delta = 0$  for an upper limit of the  $M1$  transition strength.

<sup>f</sup>Determined by the branching ratio from Ref. [17].

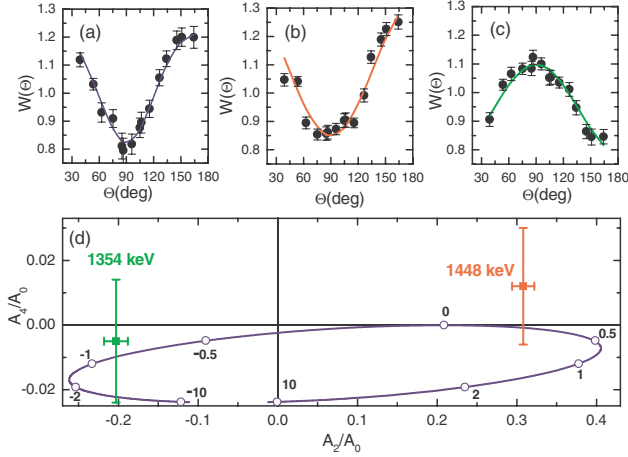


FIG. 2 (color online). Angular distribution functions for the 2237 keV (a), the 1448 keV (b), and the 1354 keV (c) transitions. The solid lines are fits to a sum of Legendre polynomials. The resulting  $A_2/A_0$  and  $A_4/A_0$  coefficients (see Table I) for the 1448 keV and the 1354 keV transitions are compared to the angular distribution ellipse (d) for  $2 \rightarrow 2$  transitions, calculated with the orientation resulting from the  $A_2/A_0$  and  $A_4/A_0$  coefficients for 2237 keV transition. The small numbers on the ellipse denote the values for the mixing ratio  $\delta$ .

yields (Table I) with respect to the  $2_1^+$  state measure the relative Coulomb excitation (CE) cross sections. These data were fitted to the Winther–de Boer theory [23] using a multiple CE code [24] and taking into account the energy loss of the beam in the target. Absolute cross sections were derived using the previously measured value for the  $B(E2; 0_1^+ \rightarrow 2_1^+) = 0.450(30)e^2b^2$  [20,25]. Unknown quadrupole moments of excited states were varied between the extreme rotational limits which introduces additional uncertainties for the matrix elements of about 2%. An unambiguous set of matrix elements  $|\langle I_f^\pi || E\lambda || 0_1^+ \rangle|$  for one-step excitations of interest was obtained. The matrix elements for the excited  $2_i^+$  states together with observed decay branching ratios  $I_\gamma(2_i^+ \rightarrow 2_1^+)/I_\gamma(2_i^+ \rightarrow 0_1^+)$  and deduced  $E2/M1$  mixing ratios for the  $2_i^+ \rightarrow 2_1^+$  transitions provide the  $B(E2)$  and  $B(M1)$  transition strengths (cf. Table I and Fig. 3).

The  $2_4^+$  state at 2.237 MeV dominates the  $2_i^+ \rightarrow 2_1^+$   $M1$  strength distribution. This identifies this level as the major fragment of the one-phonon  $2_{1,ms}^+$  state in  $^{138}\text{Ce}$ . Its one-phonon character is further corroborated by the fact that the  $2_4^+$  state exhibits the largest  $E2$  strength to the ground state after the  $2_1^+$  state. However, some parts of the  $2_{1,ms}^+$  strength are spread over nearby  $2^+$  levels. In particular, the  $2_3^+$  state at 2.143 MeV acquires a considerable  $B(M1; 2^+ \rightarrow 2_1^+)$  value. The  $2_{3,4}^+$  states are separated from the next  $2^+$  state by more than 230 keV. For further analysis of the mixing of the  $2_{1,ms}^+$  state with symmetric configurations we can, thus, consider a two-state mixing scenario between the  $2_{1,ms}^+$  MSS and a close-lying fully symmetric state (FSS). Treating the  $2_3^+$  state as a FSS is justified because the one-phonon  $2_{1,ms}^+$  state is the lowest MSS in vibrational nuclei

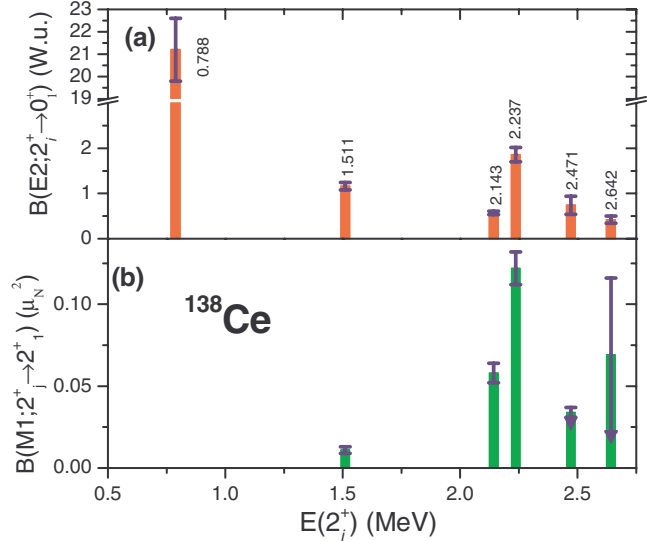


FIG. 3 (color online). (a)  $E2$  and (b)  $M1$  transition strength distributions for all observed  $2^+$  states below 2.7 MeV in  $^{138}\text{Ce}$ . The arrows indicate upper limits.

and can, thus, be surrounded only by FSSs. Since  $M1$  transitions between FSSs ( $2_1^+$  is a FSS) are forbidden by  $F$ -spin selection rules, the mixing amplitudes can be obtained from the  $M1$  strengths. This scenario leads to a mixing matrix element of 44(3) keV. The measured finite  $M1$  strength between the  $2_2^+$  and the  $2_1^+$  FSSs might indicate the presence of some  $M1$  strength from sources outside of the IBM-2 framework that one may want to take into account for arriving at even more model-independent information on the  $F$ -spin mixing matrix element. Therefore, we have extended the mixing calculations assuming that  $M1$  strength between FSSs had the size of the measured  $B(M1; 2_2^+ \rightarrow 2_1^+)$  value. In this case the mixing problem has two solutions leading to mixing matrix elements of 47 and 30 keV. As our central result we have adopted  $V_{F\text{-mix}} = 44(3)_{(-14)}^{(+3)}$  keV where the first parenthesis gives the statistical uncertainty and the second estimates systematical errors of the mixing analysis. The  $F$ -spin mixing matrix element is determined here for the first time in a procedure involving a state with predominantly mixed-symmetry character.

One might expect that excited states in the  $^{136}\text{Ba}$  and  $^{138}\text{Ce}$   $N = 80$  isotones are quite similar. The energies of the first three  $2^+$  states indeed correspond to each other within 4%. The  $2_4^+$  state at 2.129 MeV in  $^{136}\text{Ba}$  has previously been identified as a one-phonon  $2_{1,ms}^+$  state [10] and its excitation energy agrees to within 5% with the excitation energy of the  $2_{1,ms}^+$  state in  $^{138}\text{Ce}$ . However, in  $^{136}\text{Ba}$  the transition strength  $B(M1; 2_4^+ \rightarrow 2_1^+) = 0.26(3)\mu_N^2$  [10] is larger than the total  $M1$  strength  $\sum B(M1; 2_{3,4}^+ \rightarrow 2_1^+) = 0.180(13)\mu_N^2$  shared between the  $2_4^+$  and  $2_3^+$  states in  $^{138}\text{Ce}$ . Moreover, if the above mixing scenario is applied to  $^{136}\text{Ba}$ , the resulting mixing matrix element is  $<10$  keV. This drastic change in the properties of predominantly collec-

tive states points precisely to their sensitivity to the underlying subshell structure and enables us to study quantitatively the mutual balance between collective and single-particle contributions in the valence-shell isovector excitations.

In the framework of the quasiparticle-phonon model (QPM) [13], Lo Iudice and Stoyanov [12] have shown that the microscopic structure of the one-phonon FSSs and MSSs in  $^{136}\text{Ba}$  is dominated by seniority-two excitations in the  $\nu(h_{11/2})$  and in the  $\pi(g_{7/2})$  orbitals. Analogously, the leading components of two-phonon states of  $^{136}\text{Ba}$  are seniority-four excitations involving the same orbitals [12], while the three-phonon states are predominantly seniority-six excitations that require an additional proton excitation to the  $d_{5/2}$  orbital. Therefore, the one-phonon  $2^+_{1,ms}$  state of  $^{136}\text{Ba}$  has a simpler configuration than the more highly excited, predominately symmetric states that surround it around 2 MeV excitation energy. This difference in wave function complexity suppresses mixing induced by the proton-neutron residual interaction, in agreement with the experimentally determined small mixing matrix element  $V_{F-mix}(^{136}\text{Ba}) < 10$  keV.

This situation changes when going to the  $N = 80$  isotope  $^{138}\text{Ce}$ . Ground state spins for proton-odd  $N = 80$  isotones indicate the presence of a  $\pi(g_{7/2})$  subshell closure at  $Z = 58$  (cerium). Therefore, the leading one-phonon  $2^+$  proton configuration of  $^{138}\text{Ce}$  requires promotion of protons to the  $d_{5/2}$  orbital. The higher-seniority  $2^+$  states are then also formed within the same proton space as the one-phonon states. Consequently, the proton configuration of the  $2^+_{1,ms}$  state does not differ substantially from that of the nearby  $2^+$  states at 2 MeV. Residual proton-neutron interactions, such as the quadrupole-quadrupole interaction, easily lead to an enhanced mixing which concurs with our measurement of  $V_{F-mix}(^{138}\text{Ce}) = 44(3)_{-14}^{+3}$  keV.

This scenario also implies an increased neutron character for the symmetric  $2^+_1$  state at  $Z = 58$  with respect to the pure  $F$ -spin limit since the excitations within the  $\nu h_{11/2}$  orbital are energetically favorable over promotion of protons to higher orbitals. Such an asymmetry causes a reduction of the total  $M1$  transition strength between the one-phonon  $2^+$  states of  $^{138}\text{Ce}$  relative to  $^{136}\text{Ba}$ .

The proposed picture suggests that exceptionally pure one-phonon MSSs can be observed in nuclei where one-phonon states have simple configurations while, due to nearby subshell closures, multiphonon excitations must contain more involved configurations. Such situations occur when both proton and neutron numbers differ by one pair from a (sub-)shell closure, such as for the nucleus  $^{94}\text{Mo}$  [5]. This mechanism might also explain the fragmentation and strength reduction of  $2^+_{1,ms}$  states in stable Cd and Te neutron midshell nuclei, see, e.g., Ref. [26], and is expected to apply in the same way to other two-fluid quantum systems.

In summary, we have studied  $^{138}\text{Ce}$  using projectile Coulomb excitation, an experimental technique which

can straightforwardly be applied to RIBs. The data yields the  $E2$  and  $M1$  strength distributions between low spin states which reveals the  $2^+_{1,ms}$  state of  $^{138}\text{Ce}$ . In contrast to the isotone  $^{136}\text{Ba}$ , the  $2^+_{1,ms}$  state is strongly mixed with a nearby  $2^+$  FSS with a mixing matrix element of  $V_{F-mix} = 44(3)_{-14}^{+3}$  keV first measured directly for a MSS. The observed mixing in  $^{138}\text{Ce}$  can be attributed to the lack of *shell stabilization* at the proton  $g_{7/2}$  subshell closure. The evolution of the MSSs from  $^{136}\text{Ba}$  to  $^{138}\text{Ce}$  shows for the first time that the strength concentration of isovector excitations in the valence shell reflects the mutual balance between the isospin degree of freedom and the shell structure.

This work is supported by the US NSF within Contract No. PHY-0245018, by the US Department of Energy, Office of Nuclear Physics, under Contract No. W-31-109-ENG-38 and Grant No. DE-FG02-04ER41334, and by the Bulgarian NSF within Contract No. VUF-06/05.

- 
- [1] F. Iachello, Phys. Rev. Lett. **53**, 1427 (1984).
  - [2] D. Böhle *et al.*, Phys. Lett. B **137**, 27 (1984).
  - [3] O. M. Maragò *et al.*, Phys. Rev. Lett. **84**, 2056 (2000).
  - [4] E. Lipparini and S. Stringari, Phys. Rev. Lett. **63**, 570 (1989); V. O. Nesterenko *et al.*, Phys. Rev. Lett. **83**, 57 (1999).
  - [5] N. Pietralla *et al.*, Phys. Rev. Lett. **83**, 1303 (1999).
  - [6] N. Pietralla *et al.*, Phys. Rev. C **64**, 031301 (2001).
  - [7] V. Werner *et al.*, Phys. Lett. B **550**, 140 (2002).
  - [8] G. Molnár *et al.*, Phys. Rev. C **37**, 898 (1988); B. Fazekas *et al.*, Nucl. Phys. **A548**, 249 (1992).
  - [9] I. Wiedenhöver *et al.*, Phys. Rev. C **56**, R2354 (1997).
  - [10] N. Pietralla *et al.*, Phys. Rev. C **58**, 796 (1998).
  - [11] D. C. Radford *et al.*, Phys. Rev. Lett. **88**, 222501 (2002).
  - [12] N. Lo Iudice and Ch. Stoyanov, Phys. Rev. C **65**, 064304 (2002).
  - [13] V. G. Soloviev, *Theory of Atomic Nuclei: Quasiparticles and Phonons* (Institute of Physics, Bristol, 1992).
  - [14] I. Y. Lee, Nucl. Phys. **A520**, c641 (1990).
  - [15] G. M. Julian and T. E. Fessler, Phys. Rev. C **3**, 751 (1971).
  - [16] V. P. Afanasev *et al.*, Bull. Acad. Sci. USSR, Phys. Ser. (English Transl.) **35**, 1462 (1972).
  - [17] V. S. Buttsev *et al.*, Bull. Acad. Sci. USSR, Phys. Ser. (English Transl.) **38**, 54 (1974).
  - [18] J. D. Sherman, D. L. Hendrie, and M. S. Zisman, Phys. Rev. C **15**, 903 (1977).
  - [19] G. Lo Bianco *et al.*, Nucl. Phys. **A470**, 266 (1987).
  - [20] S. Raman *et al.*, At. Data Nucl. Data Tables **78**, 1 (2001).
  - [21] T. Yamazaki, Nucl. Data, Sect. A **A3**, 1 (1967).
  - [22] A. E. Stuchbery, Nucl. Phys. **A723**, 69 (2003).
  - [23] K. Alder and A. Winther, *Coulomb Excitation* (Academic Press, New York, 1966).
  - [24] H. Ower, J. Gerl, and H. Scheit, computer code CLX.
  - [25] G. Lo Bianco *et al.*, Z. Phys. A **332**, 103 (1989).
  - [26] P. E. Garrett *et al.*, Phys. Rev. C **54**, 2259 (1996); D. Bandyopadhyay *et al.*, Phys. Rev. C **67**, 034319 (2003).